DIRECT NUMERICAL SIMULATION OF MIXED CONVECTION IN TURBULENT CHANNEL FLOW: ON THE REYNOLDS NUMBER DEPENDENCY OF MOMENTUM AND HEAT TRANSFER UNDER UNSTABLE STRATIFICATION

Authors: S. Sid[+], Y. Dubief[°] and V. E. Terrapon[+]*

[+]Department of Aerospace and Mechanical Engineering, University of Liege, Liège, Belgium

[°]School of Engineering, University of Vermont, Burlington, Vermont 05405, USA

*Corresponding author: Tel: +32 4 366 92 68 Email: vincent.terrapon@ulg.ac.be

Keywords: direct numerical simulation, channel flow, mixed convection, turbulent heat transfer, unstable stratification.

ABSTRACT

Direct numerical simulations of unstably stratified turbulent channel flow have been performed in order to investigate the Reynolds number effect on mixed convection. Six different cases are considered with friction Reynolds number $\mathrm{Re}_\tau = 180$ and 395 and friction Richardson number $\mathrm{Ri}_\tau = 0, 10^2$ and 10^3. It is shown that both friction coefficient and Nusselt number increase under unstable stratification for a sufficiently large Richardson number. At low Richardson number, the friction coefficient can either increase or decrease depending on the Reynolds number. The drag reduction is associated with an increase of mean velocity due to an enhanced dissipation of Reynolds shear stress by pressure strain in the buffer region. The breakdown of the Reynolds analogy is demonstrated as the turbulent Prandtl number exhibits a non-constant behavior due to buoyancy.

NOMENCLATURE

Only uncommon symbols are defined in this section. Please refer to [1] for symbol definitions not reported hereafter.

$(\ )^+$	normalization by ν, and u_τ or T_τ
$\overline{(\ )}$	average over x, z directions and time
δ	channel half height
τ_w	mean wall shear stress $\mu(\partial\overline{U}/\partial y)_w$
u_τ	friction velocity $\sqrt{\tau_w/\rho}$
U_b	bulk velocity
Re_τ	friction Reynolds number $u_\tau\delta/\nu$
Re_b	bulk Reynolds number $U_b 2\delta/\nu$
C_f	friction coefficient $\tau_w/(1/2\rho U_b^2)$
T_h, T_c	hot and cold wall temperatures
Gr	Grashof number $g\beta(T_h - T_c)(2\delta)^3/\nu^2$
Ri_b	bulk Richardson number $\mathrm{Gr}/(\mathrm{Re}_b)^2$
Ri_τ	friction Richardson number $\mathrm{Gr}/(\mathrm{Re}_\tau)^2$
q_w	mean wall heat flux $k(\partial\overline{T}/\partial y)_w$
T_τ	friction temperature $q_w/\rho c_p u_\tau$
Nu	Nusselt number $2\delta q_w/k(T_h - T_c)$

INTRODUCTION

Understanding and predicting convective heat transfer in wall-bounded turbulent flows is of major importance in many engineering and geophysical flows. In some circumstances, convective heat transfer occurs under thermal stratification. For instance, the pressure-driven flow within a channel can be subject to buoyancy effects because of a temperature differential applied between top and bottom walls. In this situation, convective heat transfer and near-wall turbulence can be drastically affected by buoyancy where the flow dynamics results from a balance between buoyant, inertial and viscous effects. When the fluid is heated at the bottom wall and/or cooled at the top wall, the thermal stratification is unstable. Under this type of stratification, a large-scale vertical convective motion takes place within the channel. This convective motion is induced by hot and cold fluid eruptions from the walls and tends to organize the flow as longitudinal rolls. Domaradzki and Metcalfe [2] have shown through direct numerical simulations (DNS) that, depending on the Grashof number, the turbulent heat transfer can either be increased or decreased. For their lower Grashof number case ($\mathrm{Gr} < 5 \cdot 10^4$), longitudinal rolls are well organized and the heat is efficiently transported. However, an increase of buoyant effects leads to a less organized

flow and thus, a less efficient heat transfer. Furthermore, Iida and Kasagi [3] have performed DNS of unstably stratified turbulent channel flow at larger Grashof number ($9 \cdot 10^5 < \mathrm{Gr} < 4.8 \cdot 10^6$). They have shown that, for this range of Grashof numbers, the convective heat transfer efficiency monotonically increases as the Grashof number increases. In order to understand how buoyancy affects the flow dynamics, different studies have also investigated the effects of buoyancy on the near-wall turbulence in mixed convection configurations. In a non-buoyant flow, turbulence is sustained through an autonomous regeneration cycle [4] which is (i) confined to the near-wall regions and (ii) involves interactions between low- and high-speed streaks, quasi-streamwise vortices, and the mean shear. Under unstable stratification, the near-wall turbulence cycle is highly affected by the presence of the large scale convective rolls induced by thermal plumes. More precisely, the large-scale convective motion tends to confine low-speed streaks and quasi-streamwise vortices in regions where thermal plumes are generated at the wall [3]. Moreover, the ejections of low-speed streaks, associated with thermal plumes generation, are intensified by buoyancy-driven instabilities [6-7]. Besides that, the turbulent kinetic energy exchanges between the different flow regions are increased as the transport mechanisms are enhanced by natural convection [2, 5-6]. In addition, it has been shown that the quasi-streamwise vortices are weakened by the large-scale motion and the thermal plumes become the main contributor to Reynolds shear stress and turbulent heat flux generation [8-9]. Although flow dynamics of mixed convection has been subject to several valuable investigations, some important aspects have not been extensively explored. In particular, most of the studies mentioned above feature low Reynolds number turbulence ($\mathrm{Re}_\tau \leq 150$). However, the dynamics at $\mathrm{Re}_\tau = 150$ is impacted by low-Reynolds number effects [10]. One of such effect is the relative absence of log-region in the mean velocity profile for non-buoyant flows. Yet many turbulence modeling strategies implicitly or explicitly assume the existence of log-law, for example in the derivation of wall models. Another common hypothesis is the Boussinesq eddy viscosity assumption where the Reynolds shear stress is reduced to the product of an eddy viscosity with the local mean strain rate. When adequate, this approximation is only found acceptable in the log-region of the mean velocity profile. The widespread use of the eddy viscosity in turbulence modeling of mixed and forced convection flows motivates the present investigation through higher Reynolds number direct numerical simulations. The outcome is an a-priori investigation of the Boussinesq eddy viscosity assumption for the Reynolds shear stress and the gradient diffusion model for the turbulent heat flux in pressure-driven channel flow subjected to buoyancy effects.

NUMERICAL METHOD

The physical system is modeled using the incompressible Navier-Stokes equations coupled with an advection-diffusion equation for the temperature. The coupling between temperature and momentum is performed using the Boussinesq approximation:

$$\frac{\partial u_j}{\partial x_j} = 0$$

$$\frac{\partial u_i}{\partial t} + u_j \frac{\partial u_i}{\partial x_j} = -\frac{\partial p}{\partial x_i} + \frac{1}{\mathrm{Re}_\tau} \frac{\partial^2 u_i}{\partial x_j^2} + \mathrm{Ri}_\tau \, T e_y$$

$$\frac{\partial T}{\partial t} + u_j \frac{\partial T}{\partial x_j} = \frac{1}{\mathrm{Pr}\,\mathrm{Re}_\tau} \frac{\partial^2 T}{\partial x_j^2}$$

where e_y is the vertical component of the unit vector. A schematic of the simulation setup is shown in Fig. 1. The transport equations are solved over a computational domain of $4\pi\delta \times 2\delta \times 2\pi\delta$. The flow is driven by a mean pressure gradient along the streamwise direction that ensures a constant mass flow rate. Periodic boundary conditions are imposed in the streamwise (x) and spanwise (z) directions, whereas no-slip and isothermal conditions are imposed at the walls. The hot and cold temperatures are respectively associated to the bottom and top walls to induce an unstable stratification.

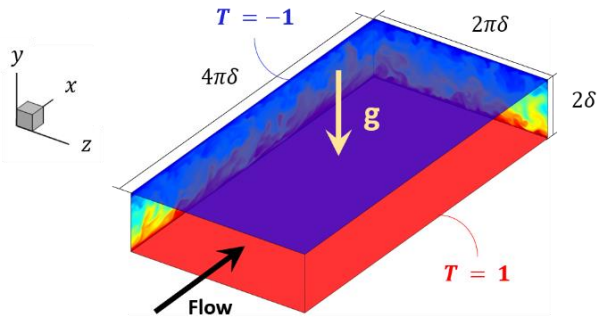

Figure 1
Schematic of the simulation setup.

The equations are advanced in time using a semi-implicit Crank-Nicolson scheme. The spatial

discretization is performed using a conservative finite difference scheme on a staggered grid [11]. The flow conditions considered are listed in Tab. 1. The mesh resolution is $512 \times 192 \times 256$ for both Reynolds numbers. Comparing this resolution with the viscous scale developed by the higher Reynolds number flow shows that the grid is fine enough to resolve the smallest scales as $\Delta x^+ \times \Delta y^+ \times \Delta z^+ = 9 \times 0.61 - 8.5 \times 9$.

Table 1
Flow conditions.

Re_τ (Re_b)	Gr	Ri_τ (Ri_b)	Pr	Case
180 (5,639)	0	0	1	P180
	$3.2 \cdot 10^6$	10^2 (0.10)	1	A180
	$3.2 \cdot 10^7$	10^3 (1.00)	1	B180
395 (13,773)	0	0	1	P395
	$1.56 \cdot 10^7$	10^2 (0.08)	1	A395
	$1.56 \cdot 10^8$	10^3 (0.82)	1	B395

RESULTS AND DISCUSSION

Macroscopic quantities: The friction coefficient and Nusselt number are reported in table 2 for the different flow conditions. Their relative changes compared to the respective passive case are shown in parentheses.

Table 2
Friction coefficient and Nusselt number. Values in parentheses are the relative changes compared to the respective passive case.

Ri_τ	C_f		Nu	
	$\mathrm{Re}_\tau = 180$	$\mathrm{Re}_\tau = 395$	$\mathrm{Re}_\tau = 180$	$\mathrm{Re}_\tau = 395$
0	0.0080	0.0065	14.6	29.4
10^2	0.0078 (−2.5%)	0.0074 (+13%)	19.7 (+35%)	45.8 (+56%)
10^3	0.0114 (+43%)	0.0091 (+40%)	34.0 (+132%)	63.3 (+116%)

For almost all the flow conditions, both friction coefficient and Nusselt number increase with growing buoyant effects. The only exception is case A180 for which the friction coefficient is slightly lower than in the passive case. A similar non-monotonic behavior has been observed by Iida and Kasagi [3] at lower Reynolds and Richardson numbers ($\mathrm{Re}_\tau = 150, \mathrm{Ri}_\tau = 40$). As a general trend, the increase in turbulent heat transfer (Nu) is more significant than the one associated with the wall shear stress (C_f). In spite of our limited parameter matrix, the low-Reynolds number effects appears to be greater on relative modification of friction coefficient and Nusselt number at lower Richardson numbers.

Mean velocity and temperature profiles: Fig. 2 shows a semi logarithmic plot of the normalized mean velocity as a function of the normalized wall distance for the different flow conditions. The linear viscous law and the law of the wall are shown as references. The mean velocity profiles (normalized by the friction velocity u_τ) corresponding to cases where the drag increases are shifted downward in all flow regions. For case A180, the mean velocity profile is shifted upward over a large flow region. This dramatic change in the shape of the mean velocity profile is associated with the drag decrease reported in the previous section. The mean velocity profile confirm our earlier speculation based on the friction coefficient and Nusselt number that the highest Richardson number is not very sensitive to low Reynolds number effects whereas the lowest Richardson number is.

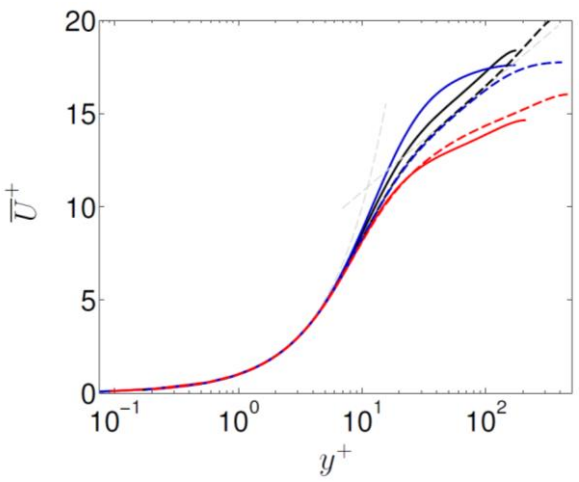

Figure 2
Mean velocity profile. P180 (—), A180 (—), B180 (—), P395 (- - -), A395 (- -), B395 (- -), $\overline{U}^+ = y^+$ (- -), $\overline{U}^+ = 1/0.41 \cdot \log(y^+) + 5.2$ (- -)

Mean temperature profiles are presented in Fig. 3. The profiles correspond to the difference between the wall and the mean temperatures normalized by the friction temperature. The mean temperature is clearly a function of both Richardson and Reynolds numbers as it is still sensitive to low Reynolds number effects even at high Richardson number. Moreover, one can see that the temperature profile exhibits an inflection point close to the centerline

which leads to negative temperature gradients in the channel center region.

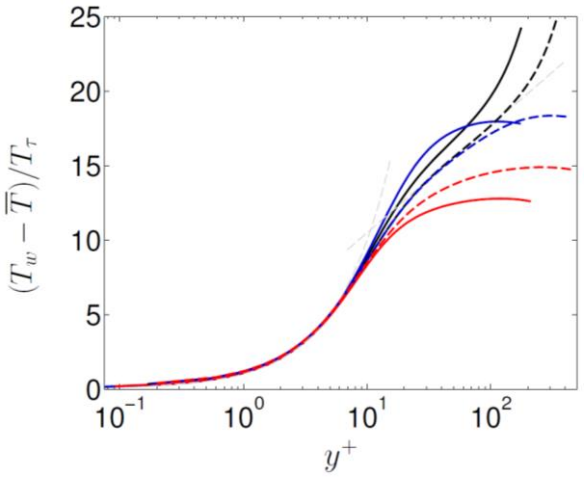

Figure 3
Mean temperature profile.
Same colour labels as in Fig. 2.
$(T_h - \bar{T})/T_\tau = 1/0.32 \log y^+ + 3.3$ (- - -)

Reynolds shear stress and turbulent heat flux distributions: Important changes are also observed for the Reynolds shear stress and the turbulent heat flux. The Reynolds shear stress distribution is shown in Fig. 4. For almost all the cases, the momentum transport by turbulence is enhanced by buoyancy as the Reynolds shear stress increases in all regions. The exception is case A180 for which the Reynolds shear stress locally decreases in the buffer layer compared to the respective passive case. As we move further from the wall, the Reynolds shear stress becomes larger than the one associated with the passive case but decreases faster such that it finally becomes smaller in the channel center region. The local decrease of Reynolds shear stress is associated with the local increase of mean velocity as the Reynolds shear stress is the turbulent transport mechanism of momentum. Although the ratio between buoyancy and inertia effects (Richardson number) is constant, buoyancy modifies the turbulence properties of the flow in a different manner depending on the Reynolds number. The turbulent heat flux distribution illustrated in Fig. 5 also supports this statement as different behaviors are observed depending on the Reynolds number considered. The transport of heat by turbulence increases in all regions as buoyancy effects increase, except for case A180 for which the turbulent heat flux is lower than for the passive case in the buffer layer. Therefore, depending on the Reynolds number, the turbulent transport of momentum and heat can either locally increase or decrease under moderate unstable stratification.

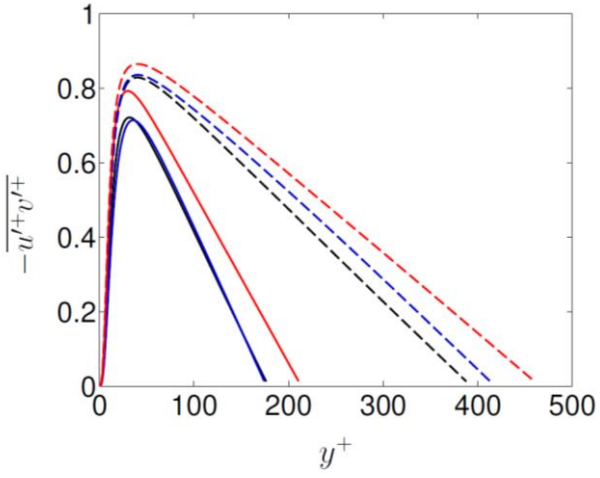

Figure 4
Reynolds shear stress.
Same colour labels as in Fig. 2.

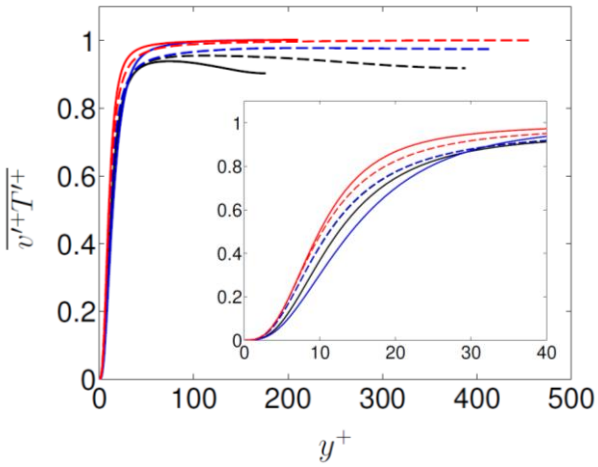

Figure 5
Turbulent heat flux.
Same colour labels as in Fig. 2.

Reynolds analogy and similarity between heat and momentum turbulent transport: The Reynolds analogy states that there exists a similarity between heat and momentum transfer for passive turbulent transport. By introducing the eddy viscosity ν_t, the Reynolds shear stress can be expressed as a function of the mean velocity gradients such as

$$-\overline{u'v'} = \nu_t \frac{\partial \overline{U}}{\partial y} \quad (1)$$

The same approach can be applied for the turbulent heat flux

$$-\overline{v'T'} = a_t \frac{\partial \bar{T}}{\partial y} \quad (2)$$

where the turbulent heat flux can be expressed as a function of the mean temperature gradients through the eddy diffusivity a_t. Then, the turbulent Prandtl number

$$\mathrm{Pr}_t = \frac{\nu_t}{a_t} = \frac{\overline{u'v'}}{\overline{v'T'}} \frac{\partial \bar{T}/\partial y}{\partial \bar{U}/\partial y} \quad (3)$$

is introduced to measure the relative differences between the momentum and heat transfer by turbulence so that the turbulent heat flux can now be expressed as a function of the eddy viscosity and the turbulent Prandtl number

$$-\overline{v'T'} = \frac{\nu_t}{\mathrm{Pr}_t} \frac{\partial \bar{T}}{\partial y} \quad (4)$$

This approach provides a simple model able to solve the averaged momentum and heat equations based on two parameters: the eddy viscosity and the turbulent Prandtl number. Fig. 6 shows the turbulent Prandtl number distribution as a function of the normalized wall distance for the different flow conditions. In RANS simulation, temperature is typically modeled using the gradient diffusion model (GFM), which, in our case, reduces to the above equation (4) with a constant Pr_t in the range 0.7 to 0.9. Fig. 6 confirms that the GFM is valid for passive scalar transport. However, the approximation experiences a dramatic breakdown for any Richardson number. Under buoyancy effects, the turbulent Prandtl number is not constant anymore and decreases as we move further from the wall. Negative values are observed in the central channel region where the temperature gradients become negative. Depending on the relative importance of the buoyant effects, the shape of the turbulent Prandtl number distribution over the wall-normal direction can be quite different. For low Richardson number, the distributions are almost linear for both Reynolds numbers. However, when buoyant effects increase, the linear behavior remains valid in the vicinity of the wall but rapidly vanishes as we move further from the wall. Furthermore, the turbulent Prandtl number converges towards a constant value in the channel center region under large unstable stratification effects whereas it still decreases for low Richardson numbers. This means that, under large buoyant effects, the discrepancy between the Reynolds shear stress and the turbulent heat flux is more significant in the near-wall region but rapidly decreases in the channel center region so that the turbulence has a similar effect on both momentum and heat transfer. Another important observation is that the turbulent Prandtl number shows a dependency on the Reynolds number. Although the shape of the curves are similar for the two Re, the slope of the linear part is larger for the low Re cases than for the large Re cases.

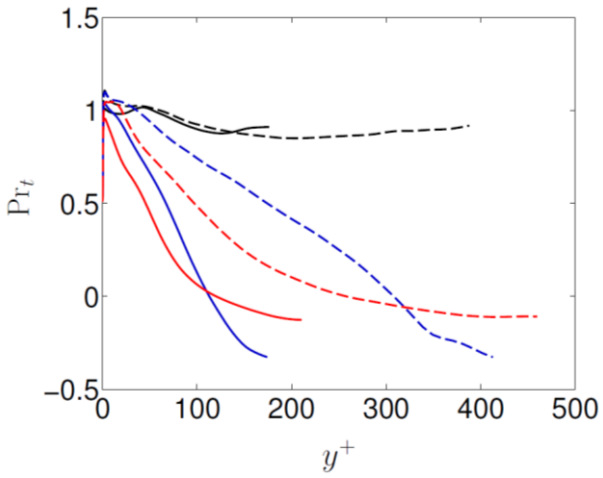

Figure 6
Turbulent Prandtl number.
Same colour labels as in Fig. 2.

Reynolds shear stress production and dissipation: The transport equations for both the Reynolds shear stress and turbulent heat flux are investigated in order to identify the changes in production and dissipation mechanisms due to buoyancy. The transport equation for the Reynolds shear stress can be written as

$$0 = \frac{\mathrm{D}\,\overline{u'^+v'^+}}{\mathrm{D}t} = \Pi_S + P_S + \varepsilon_S \quad (5)$$

where Π_S is the transport of Reynolds shear stress due to viscous, turbulent and pressure diffusion phenomena, P_S is the production of Reynolds shear stress due to both shear and buoyancy and ε is the dissipation of the Reynolds shear stress by pressure strain and viscous effects. Fig. 7 shows the difference between production P_S and dissipation ε_S along the normalized wall-normal direction for the passive and the low Richardson number cases. Although buoyancy generates additional Reynolds shear stress, a loss of shear production and an

enhanced pressure strain mechanism (not shown) leads to an increase of dissipation in the near-wall region. This additional dissipation remains significant over a large region, which is associated to the local mean velocity increase, for the low Ri case. However, combined pressure strain and viscous dissipation are not strong enough to overcome the additional buoyant production in the channel center region. As a consequence, the global production increases in this region compared to the passive case. This additional production is responsible for the decrease of mean velocity in the outer region.

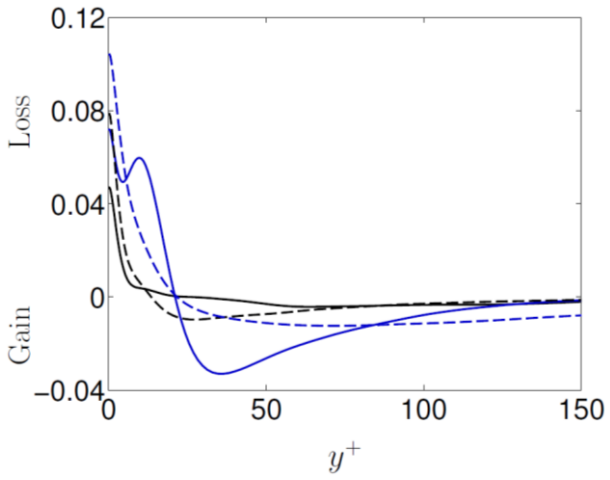

Figure 7
Budget of production and dissipation of the Reynolds shear stress $P_S + \varepsilon_S$. Same colour labels as in Fig. 2.

CONCLUSIONS

Direct numerical simulations of turbulent channel flow under unstable stratification are performed for different Reynolds and Richardson numbers. The examination of the buoyant effects on the turbulence properties leads to the following conclusions:

1. Both friction coefficient and Nusselt number increase under unstable stratification for a sufficiently large Richardson number. At low Richardson number, the friction coefficient can either increase or decrease depending on the Reynolds number.
2. The mean velocity and temperature profiles both tend to level off as buoyancy becomes important. However, the profiles can locally increase at low Reynolds and Richardson number.
3. The local increase (respectively decrease) of mean velocity and temperature profiles is associated with a decrease (respectively increase) of the Reynolds shear stress and turbulent heat flux.
4. The turbulent Prandtl number decreases along the wall-normal direction under unstable stratification. The decrease is linear for low buoyant effects while the linearity is no longer observed at large Richardson number. These observations demonstrate the breakdown of the Reynolds analogy in mixed convection.
5. The dissipation of the Reynold shear stress by the pressure-strain mechanism is enhanced by buoyancy in the near-wall region. However, this same mechanism becomes less dominant as we move further from the wall such that the Reynolds shear stress production becomes important. The production and dissipation mechanisms are also subject to a Reynolds number dependency as they result from a new equilibrium between buoyancy, inertia and viscous effects.

ACKNOWLEDGMENTS

Computational resources have been provided by the Consortium des Équipements de Calcul Intensif (CÉCI), funded by the Fonds de la Recherche Scientifique de Belgique (F.R.S.-FNRS) under Grant No.2.5020.11. We also acknowledge that the results of this research have been achieved using the PRACE Research Infrastructure resource SuperMUC based in Germany at Leibniz Supercomputing Center and MareNostrum based in Spain at Barcelona Supercomputing Center. Yves Dubief acknowledges the National Science Foundation (NSF) and Department of Energy (DOE) under grant NSF/DOE 1258697. The research leading to these results has received funding from the Fonds Spéciaux pour la Recherche of the University of Liege (Crédits classiques 2013) under grant C-13/19.

REFERENCES

1. Journal of Heat Transfer, Vol. 121, No. 4. pp 770-773, November 1999
2. Domaradzki, J. A., and Metcalfe, R. W., 1988, Direct Numerical Simulations of the Effects of Shear on Turbulent Rayleigh-Bénard Convection, Journal of Fluid Mechanics, Vol. 193, pp. 499-531.
3. Iida, O., and Kasagi, N., 1997, Direct Numerical Simulation of Unstably Stratified Turbulent Channel Flow, ASME J. Heat Transfer, Vol. 119, pp. 53-61.
4. Jimenez, J., Pinelli, A., 1999, The autonomous cycle of near-wall turbulence, Journal of Fluid Mechanics, Vol. 389, pp 335-359.

5. Lumley, J. L., Zeman, O., and Siess, J., 1978, The Influence of Buoyancy on Turbulent Transport, Journal of Fluid Mechanics, Vol. 84, pp. 581-597.
6. Fukui, K., and Nakajima, M., 1985, Unstable Stratification Effects on Turbulent Shear Flow in the Wall Region, International Journal of Heat Mass Transfer, Vol. 28, No. 12, pp. 2343-2352.
7. Mizushina, T., Ogino, F., and Katada, N., 1982, Ordered Motion of Turbulence in a Thermally Stratified Flow Under Unstable Conditions, International Journal of Heat Mass Transfer, Vol. 25, No. 9, pp. 1419-1425.
8. Fukui, K,, Nakajima, M., and Ueda, H., 1991, Coherent Structure of Turbulent Longitudinal Vortices in Unstably-Stratified Turbulent Flow, International Journal of Heat Mass Transfer, Vol. 34, No. 9, pp. 2373-2385.
9. Kasagi, N., and Iida, O., 1999, Progress in direct numerical simulation of turbulent heat transfer, Proceedings of the 5th ASME/JSME Joint Thermal Engineering Conference.
10. Moser, R.D., Kim, J., and Mansour, N., 1999, Direct numerical simulation of turbulent channel flow up to $\mathrm{Re}_\tau = 590$, Physics of Fluids, 11, pp 943-945.
11. Desjardins, O., Blanquart, G., Balarac, G., Pitsch, H., 2008, High-order conservative finite difference scheme for variable density low Mach number turbulent flows, Journal of Computational Physics, 227, pp 7125-715.